PEGylated Gold Nanoparticles: Polymer Quantification as a Function of PEG lengths and Nanoparticle Dimensions

Kamil Rahme,* [a,b,c] Timothy Doody,[d] Richard G. Hobbs, [a,b] Lan Chen [a,b,e], Michael A. Morris [a,b], Caitriona O'Driscoll,[d] and Justin D. Holmes [a,b]

[a]*Materials Chemistry and Analysis Group, Department of Chemistry and the Tyndall National Institute, University College Cork, Cork, Ireland.*

[b]*Centre for Research on Adaptive Nanostructures and Nanodevices (CRANN), Trinity College Dublin, Dublin 2, Ireland.*

[c]*Department of Sciences, Faculty of Natural and Applied Science, Notre Dame University (Louaize), Zouk Mosbeh, Lebanon*

[d]*Pharmocodelivery group, School of Pharmacie, University College Cork, Cork, Ireland.*

[e]*Department of Chemical Engineering and Biotechnology, University of Cambridge, Pembroke Street, Cambridge, CB2 3RA, UK*

*To whom correspondence should be addressed: Fax:+961 9 225164; Tel:+961 9 218950

E-mail: kamil.rahme@ndu.edu.lb

† Electronic Supplementary Information (ESI) available: [details of any supplementary information available should be included here]. See DOI: 10.1039/b000000x/

ABSTRACT:

Au nanoparticles with diameters ranging between 15 and 170 nm have been synthesised in aqueous solution using a seed-mediated growth method, employing hydroxylamine hydrochloride as a reducing agent. Thiolated polyethylene glycol (mPEG-SH) polymers, with molecular weights ranging from 2100 to 51000 g mol^{-1}, were used as efficient particle stabilising ligands. Dynamic light scattering and zeta potential measurements confirmed that the overall mean diameter and zeta potential of the capped nanoparticles increased in non linear way with the molecular weight of the mPEG-SH ligand. Electron microscopy and thermal gravimetric analysis of the polymer-capped nanoparticles, with a mean gold core diameter of 15 nm, revealed that the grafting density of the mPEG-SH ligands decreased from 3.93 to 0.31 PEG nm^{-2} as the molecular weight of the ligands increased from 2,100 to 51,400 g mol^{-1} respectively, due to increased steric hindrance and polymer conformational entropy with PEG chain length. Additionally, the number of bound mPEG-SH with a molecular weight of 10,800 g mol^{-1}, was found to increase exponentially from 278 (σ = 42) to approximately 12,960 PEG (σ = 1227) when the mean Au core diameter increased from 15 to 115 nm respectively. However, the grafting density of $mPEG_{10000}$-SH was higher on 15 nm Au nanoparticles and decreased slightly from 1.57 to 0.8 PEG nm^{-2} when the diameter increased; this effect can be attributed to the fact that smaller particles offer higher surface curvature, therefore allowing increased polymer loading per nm^2. Au nanoparticles were also shown to interact with CT-26 cells without causing noticeable toxicity.

KEYWORDS: Gold nanoparticles, stabilisation in water, PEGylation, grafting density, Cytotoxicity.

Introduction

Metal and semiconductor nanoparticles exhibit various size-dependent, optical and electronic properties that differ from the analogous bulk material.[1, 2] These properties arise due to quantum confinement effects and also due to their high surface to volume ratio.[3-5] Moreover, nanoparticles are approximately four orders of magnitude smaller than human cells, and as such they are of appropriate dimensions for applications in nanobiotechnology.[6] Particularly, nanoparticles may interact with biomolecules (e.g. enzymes, receptors, antibodies, DNA) and cells, but they are also very attractive candidates for use as carriers in medical diagnosis and treatment.[7-18] Gold (Au) nanoparticles are well known for their surface plasmon resonance band (SPR), a phenomenon associated with coherent oscillations of conduction-band electrons on the nanoparticle surface upon interaction with light.[2, 19] The wavelength of the SPR band depends from the chemical nature, size, shape and aggregation of the nanoparticles.[2, 20] Furthermore, when the nanoparticle size increases the relative contribution of scattering to the incident light extinction increases rapidly. El Sayed *et al.* [21] reported that the magnitude of light scattering by 80 nm diameter spherical Au nanoparticles was five times higher than light emission from strongly fluorescing dyes, and 40 nm nanoparticles possessed an absorption cross section five times higher than conventional absorbing dyes. Therefore, depending on their size, shape, degree of aggregation, and local environment, Au nanoparticles can absorb visible light of different wavelengths.[2, 18, 22-26] SPR bands form the basis for many biological sensing and imaging applications of Au nanoparticles.[17, 18, 22, 27-32] Moreover, Au nanoparticles are now known for their very low or zero cytotoxicity effect on cells making them useful for nanomedecine.[29, 33-38] Nanoparticles are generally unstable due to their high surface energy and can often aggregate due to the high ionic strength of many biological fluids and the non-specific interaction of nanoparticles with biomolecules, such as proteins or DNA.[39, 40] Nanoparticles are therefore usually coated by an organic capping layer thus providing a protective coating which is compatible with the solvent and counteracts the attracting forces occurring between nanoparticles causing their aggregation.[38, 41-45] Many synthetic methods have been devised to control the size and surface functionalisation of nanoparticles with the aim of maintaining their long term stability

in biological fluids.[25, 38, 46-49] Functional groups, such as mercapto (-SH), and amino (-NH_2) groups are known to have a high affinity for gold,[50] polymers having such functional groups are expected to be good stabilising agents for Au nanoparticles.[51-53] Polyethylene glycol (PEG), which is known to lengthen the circulation time of biomedicines in the bloodstream, by reducing the non-specific binding of proteins as well as the cytotoxicity, is now commonly used to coat different kinds of nanoparticles,[54] in order to improve their stability under physiological conditions and biocompatibility.[8, 55-63] However, the use of nanoparticles in biological applications requires further investigation.[64, 65] Specifically, further examination of nanoparticle size and shape distributions is required,[66] whilst an improved understanding of their surface properties is also desirable.[65, 67-69] Excess capping ligands should also be removed prior to their use in biological media in order to understand the origin of any toxicity or other side effects resulting from the introduction of nanoparticles to biological media.

This article reports on the synthesis, and polymer grafting density, of mPEG-SH-stabilised Au nanoparticles (PEG-Au), with eight different metal core diameters ranging from 15 to 170 nm. The nanoparticles were synthesised in aqueous solution using a seed-mediated growth method.[70-77] The modification of nanoparticles with PEG ligands was performed by attaching the PEG chains to the surface of the nanoparticles through a thiol linkage. Six different PEG lengths were used to modify 15 nm AuNPs with a molecular weight ranging from 2000-51000 $g.mol^{-1}$. The successful PEGylation of the nanoparticles was demonstrated using different physicochemical techniques, while the grafting densities of the various mPEG-SH ligands on the surface of the nanoparticles were estimated using a combination of electron microscopy and thermal gravimetric analysis. Finally the PEG-AuNPs were tested *in vitro* for cytotoxic effects upon interaction with CT26 cells.

Experimental

Chemicals and Materials. Purified H_2O (resistivity ≈ 18.2 MΩ cm) was used as a solvent. All glassware was cleaned with aqua regia (3 parts of concentrated HCl and 1 part of concentrated HNO_3), rinsed with distilled water, ethanol, and acetone and oven-dried before use. Tetrachloroauric acid trihydrate ($HAuCl_4,3H_2O$), sodium citrate ($C_6H_5Na_3O_7,2H_2O$), hydroxyl amine hydrochloride (NH_2OH, HCL), thiol-terminated poly(ethylene glycol) methyl ether ($\overline{M}_w$ = 2100; 5400; 10800 and 51400 g mol^{-1}) were purchased from polymer source®, while thiol-terminated poly(ethylene glycol) methyl ether ($\overline{M}_w$ = 19500 and 29500 g mol^{-1}) were purchased from Creative PEG Works. All products were used as received.

Preparation of 15 nm Diameter Gold Nanoparticles. In this study, spherical nanoparticles were obtained by reducing gold chloride in a controlled fashion. The synthesis procedure used was a modified version of the well-known and frequently used methods reported previously by Turkevich *et al*. (1951) and Frens *et al.* (1973) involving the reduction of gold chloride by sodium citrate to produce Au nanoparticles in hot water.[78, 79] The Turkevish method was revisited recently by Kimling *et al*.[77] However, in our current study very slight modifications were made to obtain monodisperse nanoparticles with low aggregation by controlling the temperature at 95 °C. 100 mL of an aqueous solution of $HAuCl_4,3\,H_2O$ (1 mmol L^{-1}) was heated to approximately 95 °C with stirring. A volume of 2.82 mL of a 170 mmol L^{-1} sodium citrate aqueous solution was rapidly added to the solution with mixing. The colour of the solution changed instantly from pale yellow to colourless, before changing to dark blue in colour after approximately 70 s, and to deep red-burgundy after 2 min. Stirring and heating of the solution was maintained for 35 min after the addition of sodium citrate. The heat was then removed and the solution was stirred upon cooling to room temperature. The nanoparticles obtained with this procedure had a mean diameter of 15 nm (σ = 1.8 nm), and the number of nanoparticles was estimated to be ~5.3×10^{15} L^{-1}, assuming that all of the initial $HAuCl_4$ was consumed in the process.

Seed-Mediated Growth of Au Nanoparticles. Large diameter gold nanoparticles were synthesised based on a previously reported seed-mediated growth method.[70, 71] In a typical procedure 0.86 mL of 0.015 mol.L^{-1} NH_2OH, HCl was added to a stirred solution of approximately 81 mL $HAuCl_4$ (0.1 mM) containing ~3 mL of citrate-stabilised Au nanoparticles (~1.6 × 10^{13} nanoparticles). The resultant nanoparticles obtained had a mean diameter of 25 nm (σ = 3.5 nm). Decreasing the number of seeds by using 2 mL of citrate-stabilised Au nanoparticles solution (~1.06 × 10^{13} Au nanoparticles) instead of 3 mL, led to an increase in the final size of the nanoparticles to approximately 32 nm (σ = 3.5 nm). Larger nanoparticles with diameters of ~65 nm (σ = 6 nm), were synthesised by using 6 mL of 32 nm diameter Au nanoparticles obtained via the procedure above, as seeds in the presence of approximately 81 mL $HAuCl_4$ (0.1 mM). Finally the ~65 nm diameter Au nanoparticles obtained previously, were used as seeds to form larger 95, 120, 130 and 170 nm diameter nanoparticles by varying the number of ~65 nm diameter Au nanoparticle seeds, for example, 14 mL ~65 nm diameter Au nanoparticle solution in the presence of 81 mL $HAuCL_4.3\ H_2O$ (0.1mM) produced nanoparticles with diameters of ~95 nm (σ = 12 nm), while decreasing the volume of the ~65 nm Au nanoparticle seeds from 14 to 6 mL yielded nanoparticles with diameters of ~130 nm (σ = 16 nm).

Grafting of Poly(ethylene glycol) Ligands. Thiolated polyethylene glycol (mPEG-SH) was covalently grafted to the surface of the Au nanoparticles. A solution of mPEG-SH of the desired molecular weight was added to a solution of citrate-capped Au nanoparticles with stirring. The solution was stirred for ~1 h allowing citrate ligands to exchange with mPEG-SH. The excess mPEG-SH was removed via centrifugation at 15 000 rpm for about 45 minutes. Thiol groups are known to have a strong affinity for Au, resulting in covalent attachment of PEG to the Au nanoparticles. The resulting colloidal solutions were very stable for several months and were able to undergo filtration and freeze drying.

Uv-visible Spectroscopy. Optical absorption spectra were obtained on a CARY UV−visible spectrophotometer with a Xenon lamp (300−900nm range, 0.5 nm resolution). The pristine 15 nm

citrate-capped Au nanoparticle solution was diluted × 3 (A ~1.2) or × 5 (A ~0.65) before measurement. Nanoparticle solutions obtained by the seeded growth method were analysed without further dilution.

Dynamic Light Scattering and Zeta Potential Measurements. The pristine solutions of Au and PEGylated Au nanoparticles, were diluted × 5 to 10 times depending on the initial concentration (absorption range 0.2- 0.5) prior to dynamic light scattering (DLS) measurements. The measurements were undertaken with the Malvern instrument (Zeta sizer Nano Series) at 25 °C using the default non-invasive back scattering (NIBS) technique with a detection angle of 173°. The model used was based on Mark Houwink parameters, all the data was fitted using the cumulant fit given by the suppliers. Three measurements were made per sample and the standard deviation (σ) was calculated, typically σ = 1-2 nm.

Transmission Electron Microscopy. Citrate and PEG-stabilised Au nanoparticles were placed on carbon-coated copper grids (Quantifoil, Germany) and dried over night in air, prior to transmission electron microscope (TEM) inspection. The samples were inspected using a JEOL JEM-2100 TEM operating at 200 kV. All the micrographs were recorded on a Gatan 1.35 K × 1.04 K × 12 bit ES500W CCD camera. TEM images were analysed using Image J software.

Scanning Electron Microscopy. Citrate and PEG-stabilised gold nanoparticles were deposited from solution on a silicon wafer and dried in air prior to inspection by scanning electron microscope (SEM). The samples were inspected using a FEI 630 NanoSEM equipped with an Oxford INCA energy dispersive X-ray (EDX) detector, operating at 5 kV.

Thermo Gravimetric Analysis. Citrate and PEG-stabilised Au nanoparticles were deposited from solution by centrifugation, and the collected Au nanoparticle material was dried at 60 °C for thermal

gravimetric analysis (TGA). TGA analysis was performed on a Mettler-Toledo TGA/DSC instrument. Samples were heated under nitrogen from 30 °C to 700 °C, at a ramp rate of 10 °C min^{-1}.

Cell Culture. The murine colon carcinoma cell line, CT26, was obtained from the American Type Culture Collection (ATCC). Cells were maintained in Dulbecco's modified Eagle medium (Sigma) supplemented with 10% fetal bovine serum (Sigma). Cells were grown in 5% CO_2 at 37°C.

MTT Cytotoxicity Assay. Cell viability was determined by the MTT assay which measures the reduction of MTT to formazan by mitochondrial reductase enzymes giving a purple colour. CT-26 cells were seeded at a density of 4×10^4 cells in a 96-well plate and grown in complete medium for 24 hr. Au NPs were added to the cells and incubated for 4 hr. The medium was removed and was replaced with fresh complete medium containing MTT ((3 - (4,5-dimethylthiazole-2-yl) -2,5-diphenyl tetrazolium) bromide) (Sigma) at a working concentration of 0.5 mg ml^{-1}. After 4 hr incubation, cell culture medium was removed, and the formazan crystals produced were dissolved in 100 µl of DMSO for 5 min at room temperature. Absorbance was read at a wavelength of 590 nm. All experiments were carried out in triplicate.

Results and Discussion

Chemical Synthesis of Au Nanoparticles.

Chemical reduction of Au salts, usually $HAuCL_4.3H_2O$, is widely used for the synthesis of Au nanoparticles.[19, 33, 80-82] Recently Polte *et al.* described a four step mechanism for the formation of Au nanoparticles obtained by citrate reduction of $HAuCl_4$ using in-situ nanoparticle growth monitoring via XANES and SAXS.[81] Additionally, Ji *et al*. have described two mechanisms for the formation of Au nanoparticles with citrate, based on the solution pH, whereby Au nanoparticles form by fast, random particle attachment and ripening for solutions with pH < 6.5, whilst slower nucleation and ripening was observed for synthesis solutions with pH 6.5-7.7. The role of citrate as a pH mediator was also

identified by Ji *et al.*[83] The method outlined herein allowed synthesis of 15 nm Au nanoparticle seeds by chemical reduction of $HAuCl_4$ with sodium citrate at pH < 6.5 and at a temperature of 95 °C, suggesting that the first mechanism outlined by Ji *et al.* can be applied here thus allowing fast formation of Au nanoparticles. Larger Au nanoparticles were produced by the seeding method, which involved adding Au seed particles (prepared by the method described above) to $HAuCl_4.3H_2O$ in the presence of a weak reducing agent such as hydroxylamine hydrochloride. The latter does not act to induce Au nanoparticle seed aggregation, but only acts as a growth agent in slightly acidic conditions. Therefore, the reduction of $HAuCl_4$ with hydroxylamine hydrochloride in the presence of Au nanoparticles yields an increased population of the seeds by surface catalysed reduction of $HAuCl_4$. [2, 70, 71, 74, 75, 84] Polydispersity and diverse shape formation was reduced during synthesis, by growing the nanoparticles in a stepwise fashion. 15 nm diameter citrate capped Au nanoparticles were first ripened to ~23 nm and subsequently ~32 nm in diameter. The ~32 nm diameter particles were then ripened to ~65 nm in diameter and subsequently to larger diameters (~93 nm, 115 nm, 135nm, and 175 nm) by varying the concentration of the nanoparticle seeds.

Au nanoparticles prepared in this study were characterized by UV−Visible absorption spectroscopy **(Figure 1(a))** and either TEM or SEM **(Figure 2).** Four parameters were used to describe each preparation of colloids: the wavelength of maximum absorbance (λ_{max}) and the peak width at the base ($\Delta\lambda$) from the UV−Vis absorption spectra, and the mean particle diameter (*d*) and circularity (C) from electron microscopy analysis. The results from the characterisation by UV-visible and EM for all the nanoparticles used in this study are given in **table 1.** The UV-visible spectra clearly show a red shift in the plasmon absorbance band with increasing Au nanoparticle diameter. The observed red shift is accompanied with a further broadening of the absorbance band. The band width (λ_0) was found to increase from 98 to 342 nm when the mean nanoparticle diameter increased from 30 to 135 nm, which can be explained by the fact that higher oscillation modes (quadrupole, octopole absorption and scattering) also affect the extinction cross section with increasing size. Therefore the plasmon

absorption maximum (λ_{max}) is shifted to a higher wavelength and the bandwidth increases.[2] However, when the size of the nanoparticles increases to 170 nm the plasmon absorption band is split into two peaks with the first centred at ~560 nm and the second centred at ~790 nm. Scattered light becomes more dominant in the absorption spectra for larger nanoparticles, and this can be seen clearly in spectra obtained from nanoparticles with diameters of ~170 nm as shown in figure 1**.** The electron microscopy images in figure 2 show that the nanoparticle diameter distribution widths and circularity were not strongly affected by increasing diameter and therefore comparable diameter distribution widths and nanoparticle circularity to the initial seeds were observed. Histograms of the nanoparticle diameters as obtained from TEM image analysis using *Image J* software are included in the supporting information. Au nanoparticles are electrostatically stabilised and as such they are very sensitive to any change in the ionic strength and/or pH of the medium in which they are dispersed, which can induce nanoparticle aggregation. PEG is known to improve the stability and biocompatibility of the nanoparticles, and has been used to coat the nanoparticles directly after preparation. The current strategy was to attach PEG polymers to Au nanoparticles through Au-SH chemical bonding. PEG attachement to the nanoparticles causes a very slight red shift of about 2 nm in the plasmon absorption bands **(**figure 1 (b)**)** due to a change of the dielectric constant at the nanoparticle surface. The successful PEGylation of Au nanoparticles was proven by dynamic light scattering and zeta potential measurements.

Dynamic Light Scattering (DLS).

Electron microscopy analysis of Au nanoparticles requires preparation of a dried nanoparticle specimen, consequently, electron microscopy analysis does not allow inspection of the dimensions of nanoparticles as they exist in solution. DLS, also known as photon correlation spectroscopy (PCS), or quasi-elastic light scattering, is a suitable and sensitive technique for the characterisation of dispersions of nanoparticles and nanoparticle-polymer hybrids. DLS not only provides a route to measure particle size distributions, but also protein (and other biomolecule) molecular weight distributions in solution.[85] PEG is a flexible linear polymer. Consequently, PEG can dramatically influence the Brownian motion

of particles by introducing additional frictional drag and thus reducing nanoparticle diffusivity. The combined use of electron microscopy techniques and DLS can provide a full physical characterisation of colloidal dispersions of Au nanoparticles for biomedical applications. In the present study, ~15 nm Au nanoparticles were coated with different molecular weights of mPEG-SH and the hydrodynamic diameter were measured by DLS. **Figure 3(a)** shows the size distribution of the Au nanoparticles before and after coating. One can clearly see an increase in the mean nanoparticle diameter from ~20 nm for 'bare' citrate capped Au nanoparticles to ~105 nm for a mPEG-SH molecular weight of 48,000 g mol^{-1}. The zeta potential was also observed to shift from around -35 mV for citrate capped Au nanoparticles, to ~ -1 mV for Au nanoparticles with a mPEG-SH molecular weight of 20,000 g mol^{-1}. The zeta potential measurements displayed in **Figure S2** (see figure S2 in supporting information) prove that the nanoparticles were successfully coated with a neutral capping layer. **Figure 3(b)** shows a plot of nanoparticle diameter (D_h), and zeta potential against the molecular weight of the mPEG-SH polymer. The diameter D_h was calculated by Z average obtained through the Cumulant method using DLS. The solid lines shown in figure 3(c) are exponential fits to the experimental data, where a near linear increase is shown for mPEG-SH in the molecular weight range 2,100-10,800 g mol^{-1}, before a plateau appears for mPEG-SH with higher molecular weight (M_w ~ 19,500, 29,500 and 51,400 g mol^{-1}). The mPEG-SH layer thickness was estimated from the diameter distribution by volume from DLS and the values are given in table 2**.** The hydrodynamic diameter increases with PEG length, and leads to a complimentary decrease in the absolute zeta potential from -35 to -1 mV. The observed decrease in the zeta potential values with increased mPEG-SH molecular weight is not suprising as the zeta potential values are measured at the surface plane of the hydrodynamic sphere of diameter (D_h). The surface plane of the hydrodynamic sphere is far from the surface of the Au nanoparticles. Perrault *et al.* have reported that the hydrodynamic diameter of 50 nm diameter citrate capped Au nanoparticles increased after PEGylation with $mPEG_{5000}$-SH until saturation at a surface coverage of 5-10 PEG nm^{-2}. Similarly the absolute zeta potential decreased from -31.1 mV (citrate capped Au nanoparticles) to -7.2 mV (5 PEG nm^{-2}).[76] The exponential increase in the nanoparticle diameter with PEG length observed here has led to

the hypothesis that fewer polymers can be loaded on ~15 nm nanoparticles when the size of the polymer increases due to strong sterical hindrance, therefore the grafting density (number of PEG nm^{-2}) of mPEG-SH to Au nanoparticles depends on the length of the polymer. Consequently, verification of this hypothesis required quantification of the number of PEG molecules grafted to each nanoparticle. Au nanoparticles of various mean diameters, coated with $mPEG_{10,000}$-SH, were selected to study the effect of nanoparticle diameter on mPEG-SH grafting density. **Figure 4** shows the diameter distribution by intensity of Au nanoparticles with mean diameters of 15, 30, 65, 95, 115, and 170 nm coated with $mPEG_{10000}$-SH. The zeta potential of all the Au nanoparticles coated with $mPEG_{10000}$-SH was in the range -7 to -1 mV. The grafting density of $mPEG_{10000}$-SH to Au nanoparticles was estimated using TGA.

Quantification of PEG loaded onto Gold Nanoparticles using Thermo Gravimetric Analysis (TGA).

The number of mPEG-SH molecules grafted to each Au nanoparticle was estimated by performing thermal gravimetric analysis measurements. The nanoparticles were isolated by centrifugation, and dried prior to TGA. TGA was performed by heating the nanoparticle powder from 30 to 700 °C under N_2. The weight loss seen during the heating process corresponds to degradation of the organic material in the sample. A PEG polymer standard was observed to degrade at a temperature lower than 300 °C, whilst the PEGylated nanoparticles appeared to degrade at higher temperatures (300-500 °C) (see figure S3 in supporting information). **Figure S3(b)** shows the first derivative of the weight loss as a function of temperature for the free polymer mPEG-SH (Mw ~10000 g mol^{-1}), and the sample of 30 nm Au nanoparticles functionalised with $mPEG_{10\,000}$-SH after purification. The data in figure S2 clearly shows that the free polymer degrades between 200 and 300 °C, while the grafted polymer degrades at higher temperature, most likely due to the fact that more energy is needed to cleave the Au-S bond, and the expected local increase in PEG density at the Au nanoparticle surface relative to the free PEG polymer in the standard sample. A single centrifugation was performed prior to TGA in order to avoid significant stress on the monolayer of PEG at the nanoparticle surface that may lead to release of

attached PEG. Additionally, weight loss below 300 °C during TGA was not taken into account for the calculation of the PEG grafting density (see supporting information). The weight loss between 320 and 460 °C was supposed to correspond to the thermal decomposition of the attached PEG moieties at the surface of the nanoparticles.[86] TGA was performed on ~15 nm Au nanoparticles coated with PEG of different lengths as well as for $mPEG_{10,000}$–SH coated Au nanoparticles with diameters of 15, 30, 65, 95, and ~115 nm. The number of PEG molecules grafted to each Au nanoparticle was estimated by considering the TGA weight loss data and assuming a spherical nanoparticle shape. An example of the calculation to derive the PEG grafting density is included in the supporting information. Table 2 shows the results of TGA and DLS analysis for 15 nm Au nanoparticles coated with mPEG-SH of various molecular weight, as well as the calculated grafting density of mPEG-SH for each molecular weight. Table 3 presents the experimental results of TGA and DLS analysis for $mPEG_{10\ 000}$–SH coated Au nanoparticles with various Au nanoparticle diameters. **Figure 5(a)** shows a plot of the number of mPEG-SH molecules grafted on ~15 nm Au nanoparticles as a function of the molecular weight of the polymer. The number of PEG molecules grafted to the Au nanoparticles decreased with increasing PEG molecular weight. Specifically, the number of PEG molecules grafted to the Au nanoparticles decreased by ~12 fold from 695 ± 87 for $mPEG_{2,000}$-SH (3.93 PEG nm^{-2}) to 50 ± 6 for $mPEG_{48,500}$-SH (0.317 PEG nm^{-2}). The solid line is an exponential fit to the data. Increased conformational entropy of the PEG molecules with polymer chain length leads to an increase in the footprint of the PEG molecules at the Au nanoparticle surface from 0.25 nm^2 for $mPEG_{2,000}$-SH to 3.15 nm^2 for $mPEG_{48,500}$-SH (see table 2). The effect of increased PEG chain length on grafting density is shown schematically in the cartoon in figure 5(a). A similar trend has been observed by Shi *et al*. where they reported that the grafting density on PEGylated 92.5 nm ninosomes with M_w 2, 5 and 10 KDa was 0.53, 0.45 and 0.17 PEG nm^{-2} respectively.[87] Wulfing *et al*. found that $mPEG_{5,000}$-SH has a footprint of 0.35 nm^2 on 2.8 nm diameter Au nanoparticles,[88] while Takae *et al*. found that the number of PEG molecules, a mixture of (acetal-PEG-S-)$_2$ and (lactose-PEG-S-)$_2$ with molecular weights of 12,000 and 12200 g mol^{-1} respectively, grafted on 20 nm diameter Au nanoparticles was 520 molecules per nanoparticle by TGA.[86] **Figure**

5(b) shows a plot of the number of $mPEG_{10,000}$–SH molecules measured per nanoparticle by TGA as a function of the mean nanoparticle diameter (measured by TEM/SEM). The number of $mPEG_{10,000}$–SH ligands per nanoparticle was observed to increase from 278 ligands per 15 nm diameter Au nanoparticle, to ~12,960 ligands per 115 nm diameter Au nanoparticle. A similar observation was made by Hurst *et al*. for fluorescent DNA-PEG-SH ligands,[89] and Maus *et al*. using fluorescence based peptide assay to quantify the number of amino groups grafted on Au nanoparticles capped with a mixed self-assembled monolayer of SH-$PEG_{3,000}$-NH_2 and SH-$PEG_{3,000}$-COOH.[90] Finally, some similar behaviour has been observed in this work where the grafting density of $mPEG_{10,000}$-SH was higher on 15 nm diameter Au nanoparticles and decreased slightly from 1.573 to 0.8 PEG nm^{-2} when the particle size increased to 65 nm in diameter (table 3). The fact that smaller Au nanoparticles display a higher density of thiol ligand attachment has been attributed to their high surface curvature.[91]

Conformation of the PEG polymers on the AuNPs surface. The Flory radius (F) described as ($F=\alpha n^{3/5}$) where n is the number of monomers per polymer chain and α is the length of one monomer in Angstroms (α = 3.5 Å for PEG),[54, 92, 93] give the information about the two main conformations 'mushroom' and 'brush' that PEG chains can acquire depending on grafting density. The 'mushroom' conformation is known to occur for low surface density mainly when the distance D, between the attachment points of polymer to a surface is larger than F (D > F). In contrast the 'brush' conformation is observed when D < F. However, a transition of mushroom to brush conformation can take place when the value of D becomes close to F.[94] The value of D was estimated here and none of the values of D was found to be greater than F (see supporting information). Therefore, we can conclude that is this study the 'brush' conformation is the only obtained conformation, even though that the PEG grafting density and foot print were found to varies the PEG chain length. The results shown here are not surprising, as in our system, the grafting site is a single covalent bond, and a **s**trongly stretched situation for a grafted layer in water as a good solvent is favourable.[93] Furthermore and an excess of polymer is added in the beginning, a well separated irreversibly grafted chains (mushroom regime) cannot easily obtained as maximum of

polymers were loaded on the surface of gold nanoparticles. Finally, it is well known that denser packing can be achieved on the curved surface of AuNPs compared to that on a flat substrate due to a reduction in steric hindrance as the free end of the PEG molecules are less confined.[95, 96]

Cytotoxicity on CT26 cells.

The viability of CT26 cells after treatment with the Au nanoparticles was determined by the MTT assay. Cells were treated with a range of Au nanoparticles at biologically active concentrations **(Figure 6).** None of the PEG-Au nanoparticles synthesised in this study exhibited any cytotoxicity in CT-26 cell cultures.

Conclusions

We have synthesised nearly spherical Au nanoparticles with a wide range of diameters (15 to 170 nm), and narrow diameters distributions (10 - 15 %) using a controlled seed mediated growth approach. The Au nanoparticles show size dependent optical properties making them very suitable for further applications (*e.g.* photonic and bioimaging). Different molecular weights of PEG were used to modify the Au nanoparticle surface. 15 nm diameter Au nanoparticles coated with mPEG-SH of various molecular weights has been shown to lead to an exponential increase in the nanoparticle diameter in solution. Additionally, increasing PEG polymer chain length has been observed to effectively increase screening of the negative Au nanoparticle charge. Quantification of the number of PEG molecules grafted per nanoparticle shows that the grafting density decreases in non linear way with the PEG length due to increased conformational entropy of the polymer with chain length. Similarly, the grafting density of $mPEG_{10,000}$-SH was shown to decrease slightly with increasing Au nanoparticle diameter, while the number of polymers grafted was found to increase in non linear way with the size. As the colloidal stability with PEG is known to offer a stealth character and now is high of interest for biomedical application. This full study on synthesis, stabilisation and characterisation of PEGylated nanoparticles in water, using a wide range of PEG molecular weight with one nanoparticle size and on a

wide range of gold nanoparticles sizes with mPEG$_{10,000}$-SH, as well as their stability in biological media and very poor cytotoxicity make these particles suitable for use in further biological studies. Finally, this study presented here may be very helpful for researchers interested in grafting biomolecules (drugs, protein, peptide, etc.) through a chemisorbed PEG spacer on nanoparticles, as our results may gives them a rough idea about the quantity of PEG-biomolecules (in theory supposed to be slightly lower than the neutral mPEG used here) that can be loaded on nanoparticles in water. The low toxicity of AuNPs and proven ability of the PEGylated nanoparticles to offer a stealth character indicates the potential of Au NP's for bioconjugation to active targeting and receptor mediated delivery *in vivo*.

ACKNOWLEDGMENT We acknowledge financial support from Science Foundation Ireland (Grant 07/SRC/B1155 and 07/SRC/B1154) to the Irish Drug Delivery network (IDDN) through Strategic Research Cluster (SRC) grants. This research was also enabled by the Higher Education Authority Program for Research in Third Level Institutions (2007-2011) via the INSPIRE programme. Microscopy analysis was undertaken at the Electron Microscopy and Analysis Facility (EMAF) at the Tyndall National Institute, Cork, Ireland.

FIGURES

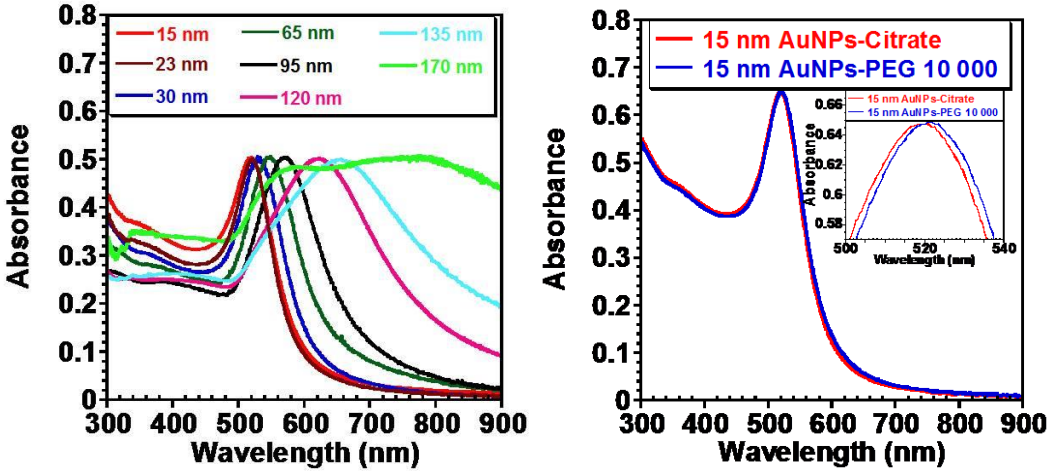

Figure 1. (a) UV-visible spectra of different AuNPs sizes synthesized in this study (absorbance adjusted to the same value). (b) Spectra of 15 nm AuNPs before and after PEGylation, the inset show the clear red shift of about 2 nm after PEGylation.

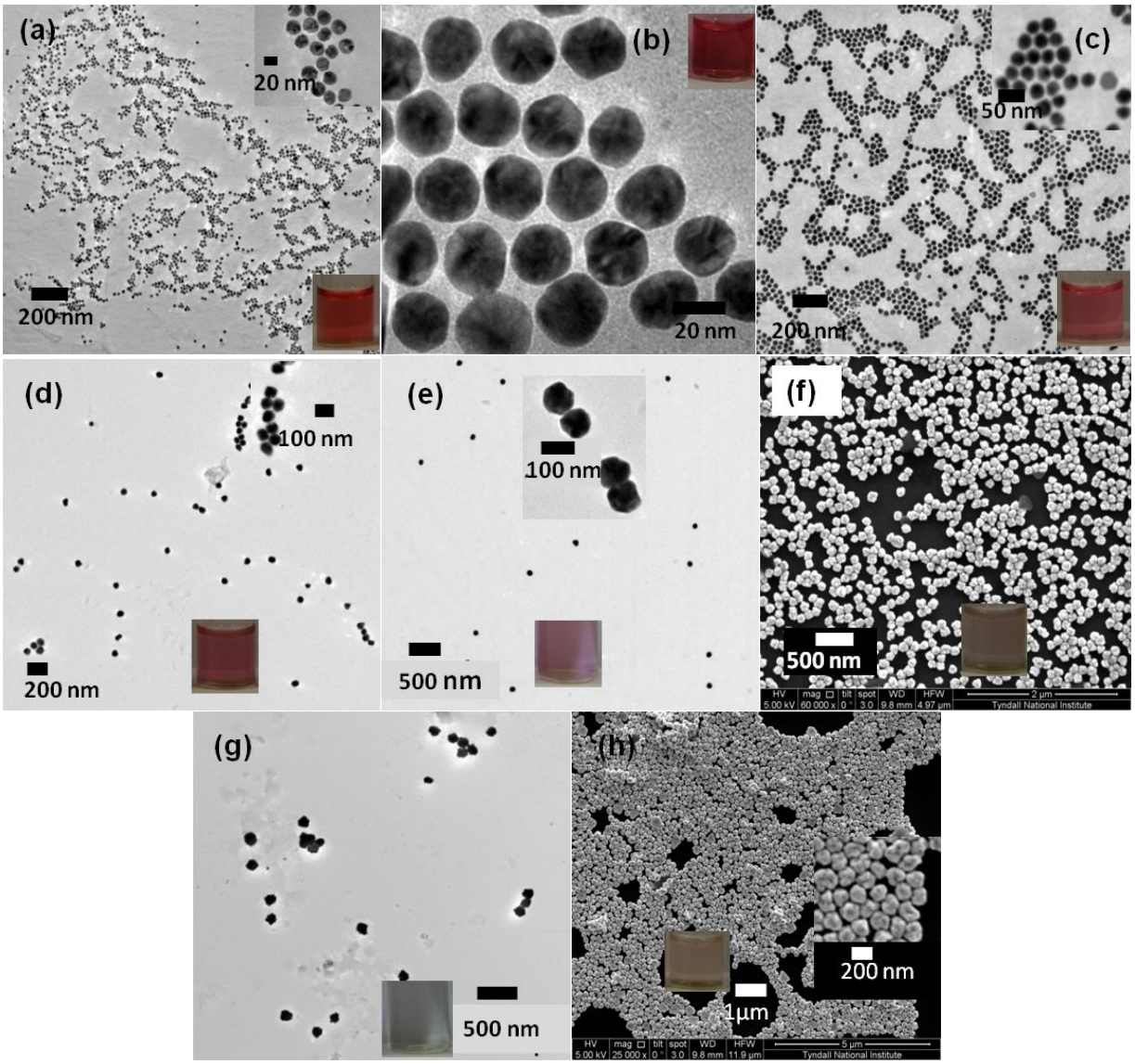

Figure 2. TEM micrographs of Au nanoparticles produced in this study with mean diameters of (a) ~15 nm (b) ~ 23 nm, (c) ~30 nm (d) ~ 63 nm (e) ~93 nm and (g) ~135 nm. SEM images of Au nanoparticles with diameters of (f) ~115 nm (h) ~170 nm. The insets show higher magnification electron micrographs, and optical photographs of the the corresponding colloidal solutions.

Table 1. Characteristic data's from UV-visible and EM results for all the nanoparticles used in this study.

Diameter (nm)	Standard dev	λ_{max} (nm)	$\Delta\lambda$ (nm)	Circularity	Standard dev
15	1.8	519	90	1.06	0.1
23	3.5	521	84	1.12	0.08
30	4	525	98	1.15	0.11
62.5	6	546	134	1.16	0.1
93	12	568	165	1.14	0.1
115	10	620	261	1.15	0.14
134	16	654	342	1.18	0.13
170	20	2 picks	>350	1.2	0.15

Parameters characteristics (Plasmon position, peak width, diameter and circularity) data's for the particles prepared in this study extracted from UV-visible and microscopy analysis.

(a)

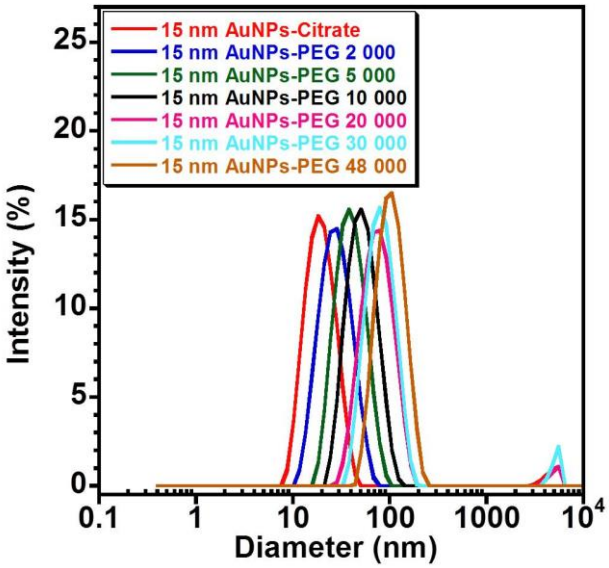

(b)

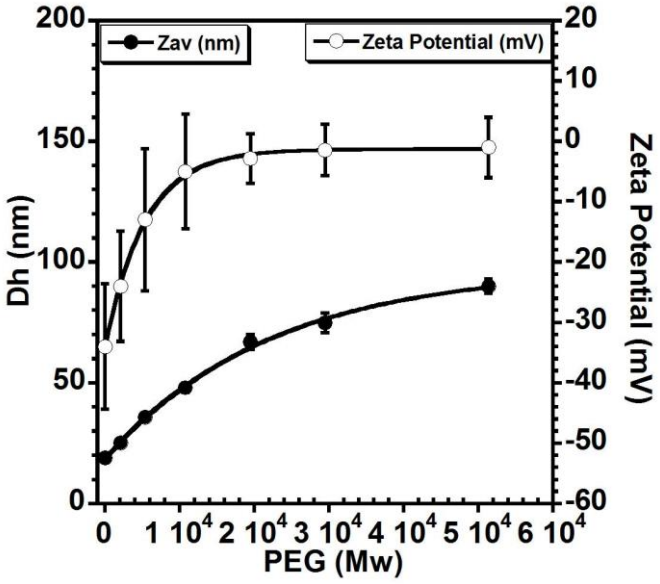

Figure 3. (a) Size distribution by intensity of approximately 15 nm AuNPs coated with mPEG-SH of different molecular weight. (c) Evolution of the hydrodynamic diameter (Y left axis) and Zeta Potential (Y right axis) in function of the molecular weight (D_h is given by Zav obtained through the Cumulant method from DLS measurements) the solid lines correspond to a fit of the experimental values.

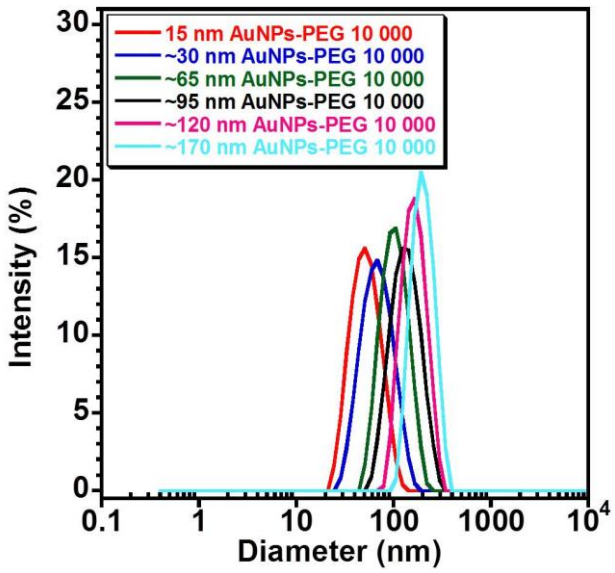

Figure 4. Size distribution by intensity of different AuNPs sizes coated with the $mPEG_{10\ 000}$-SH (~245 EO units).

(a) (b)

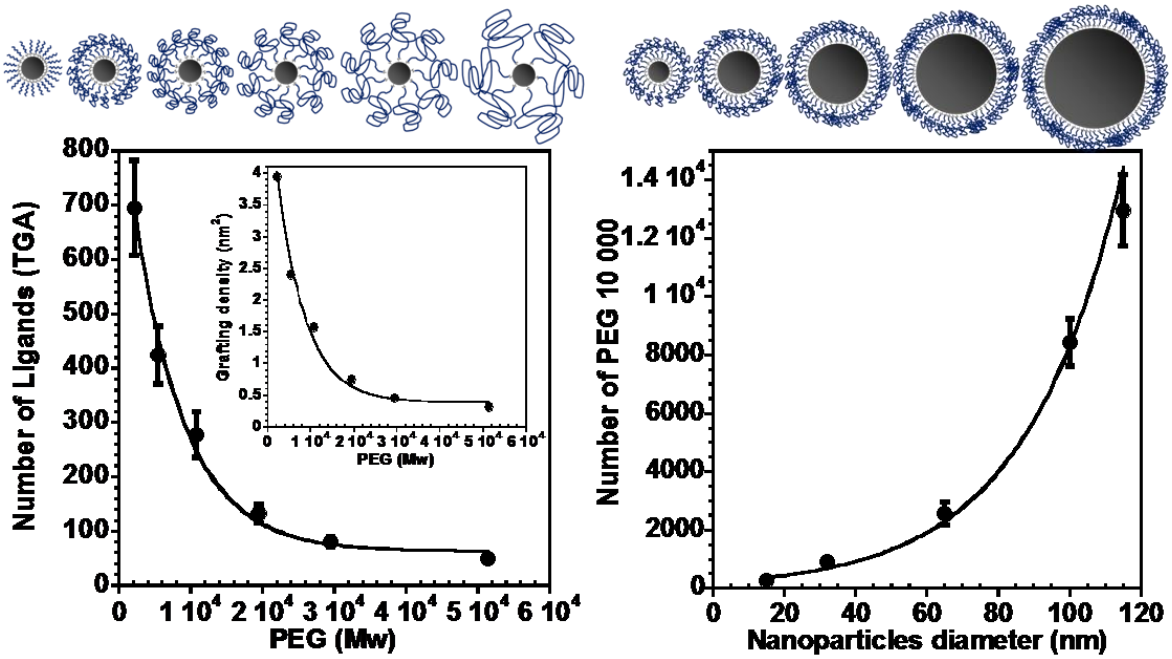

Figure 5. (a) Possible schematisation and the number of ligands (mPEG-SH) on 15 nm AuNPs estimated from TGA in function of the molecular weight, inset shows the grafting density. (b) Possible schematisation and number of $mPEG_{10\,000}$-SH estimated from TGA in function of the AuNPs diameter.

Table 2. Surface Coverage (from TGA) and mPEG-SH layer thickness (from DLS size distribution by volume) on 15 nm Gold Nanoparticles.

mPEG-SH (Mw)	Number of EO	DLS (v)/PEG layer (nm)	Weight Loss (%) T>320 °C	N_{PEG} per 15 nm AuNP	Foot Print (nm^2)	Grafting density/ nm^2
2100	47	2.83 ±0.66	6.7	695± 87	0.25	3.93
5400	122	7.79 ± 1.0	9.9	424± 53	0.42	2.4
10 800	245	12.77 ± 1.5	12	278±42	0.63	1.57
19 500	443	21.61 ± 2.5	10.82	132 ± 16.5	1.33	0.75
29 500	670	25.6 ± 3.0	10	81± 10	2.18	0.46
51400	1168	37.15 ± 4.0	10.85	50 ± 6	3.15	0.32

Table 3. Surface Coverage (from TGA) of different AuNPs diameter (EM/DLS) coated with $mPEG_{10\,000}$-SH

Diameter (nm)/EM	Diameter (nm)/DLS (I)	Weight Loss (%) T>320 °C	N_{PEG} /AuNP	Foot Print (nm^2)	Grafting density/ nm^2
15 ± 1.8	59 ± 3.5	14.25	278 ± 42	0.63	1.57
30 ±3.5	72 ± 5	5.7	916 ± 106	0.78	1.29
62.5 ± 6	102 ± 9	1.64	2572 ± 402	1.25	0.8
93 ± 12	138 ± 10	1.41	6778 ± 814	1.05	0.96
115 ± 10	165 ± 14	1.449	12960 ± 1227	0.8	1.25

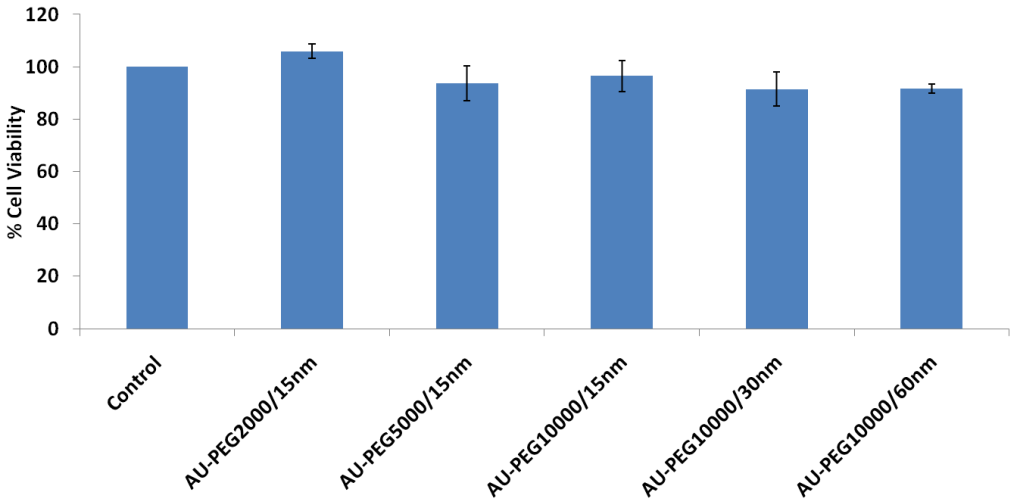

Figure 6. Percent of Cell viability in CT-26 cells following AuNPs-PEG treatment relative to control untreated cells (analyzed by MTT assay)

REFERENCES

1. P. D. C. N. R. Rao, P. D. G. U. Kulkarni, P. John Thomas and P. D. Peter P. Edwards, *Chemistry - A European Journal*, 2001, **8**, 28-35.
2. S. Link and M. A. El-Sayed, *Journal of Physical Chemistry B*, 1999, **103**, 4212-4217.
3. S. Abe and K. Kajikawa, *Physical Review B*, 2006, **74**, -.
4. H. Bonnemann and K. S. Nagabhushana, *Journal of New Materials for Electrochemical Systems*, 2004, **7**, 93-108.
5. C. Bouvy, F. Piret, W. Marine and B. L. Su, *Chemical Physics Letters*, 2007, **433**, 350-354.
6. G. M. Whitesides, *Nature Biotechnology*, 2003, **21**, 1161-1165.
7. J. Q. Wang, M. H. Sui and W. M. Fan, *Current Drug Metabolism*, 2010, **11**, 129-141.
8. X. M. Qian, X. H. Peng, D. O. Ansari, Q. Yin-Goen, G. Z. Chen, D. M. Shin, L. Yang, A. N. Young, M. D. Wang and S. M. Nie, *Nature Biotechnology*, 2008, **26**, 83-90.
9. D. Peer, J. M. Karp, S. Hong, O. C. FaroKHzad, R. Margalit and R. Langer, *Nature Nanotechnology*, 2007, **2**, 751-760.
10. M. Arruebo, M. Valladares and A. Gonzalez-Fernandez, *Journal of Nanomaterials*, 2009, -.
11. H. M. E. Azzazy, M. M. H. Mansour and S. C. Kazinierczak, *Clinical Biochemistry*, 2007, **40**, 917-927.
12. P. Baptista, E. Pereira, P. Eaton, G. Doria, A. Miranda, I. Gomes, P. Quaresma and R. Franco, *Analytical and Bioanalytical Chemistry*, 2008, **391**, 943-950.
13. P. H. Chou, S. H. Chen, H. K. Liao, P. C. Lin, G. R. Her, A. C. Y. Lai, J. H. Chen, C. C. Lin and Y. J. Chen, *Analytical Chemistry*, 2005, **77**, 5990-5997.
14. V. Dixit, J. Van den Bossche, D. M. Sherman, D. H. Thompson and R. P. Andres, *Bioconjugate Chemistry*, 2006, **17**, 603-609.
15. R. Guo, L. Y. Zhang, H. Q. Qian, R. T. Li, X. Q. Jiang and B. R. Liu, *Langmuir*, 2010, **26**, 5428-5434.
16. A. Hoshino, S. Hanada, N. Manabe, T. Nakayama and K. Yamamoto, *Ieee Transactions on Nanobioscience*, 2009, **8**, 51-57.
17. X. H. Huang, P. K. Jain, I. H. El-Sayed and M. A. El-Sayed, *Lasers in Medical Science*, 2008, **23**, 217-228.
18. X. H. Huang, S. Neretina and M. A. El-Sayed, *Advanced Materials*, 2009, **21**, 4880-4910.
19. M. C. Daniel and D. Astruc, *Chemical Reviews*, 2004, **104**, 293-346.
20. C. J. Murphy, T. K. San, A. M. Gole, C. J. Orendorff, J. X. Gao, L. Gou, S. E. Hunyadi and T. Li, *Journal of Physical Chemistry B*, 2005, **109**, 13857-13870.
21. Prashant K. Jain, Kyeong Seok Lee, Ivan H. El-Sayed and a. M. A. El-Sayed, *J. Phys. Chem. B*, 2006, **110**, 7238-7248.
22. K. S. Lee and M. A. El-Sayed, *Journal of Physical Chemistry B*, 2006, **110**, 19220-19225.
23. K. L. Kelly, E. Coronado, L. L. Zhao and G. C. Schatz, *Journal of Physical Chemistry B*, 2003, **107**, 668-677.
24. A. M. Schwartzberg, T. Y. Olson, C. E. Talley and J. Z. Zhang, *Journal of Physical Chemistry B*, 2006, **110**, 19935-19944.
25. K. Rahme, F. Gauffre, J. D. Marty, B. Payre and C. Mingotaud, *Journal of Physical Chemistry C*, 2007, **111**, 7273-7279.
26. S. Eustis and M. A. El-Sayed, *Chemical Society Reviews*, 2006, **35**, 209-217.

27. M. Hu, J. Y. Chen, Z. Y. Li, L. Au, G. V. Hartland, X. D. Li, M. Marquez and Y. N. Xia, *Chemical Society Reviews*, 2006, **35**, 1084-1094.
28. P. K. Jain, X. H. Huang, I. H. El-Sayed and M. A. El-Sayed, *Accounts of Chemical Research*, 2008, **41**, 1578-1586.
29. N. G. Khlebtsov and L. A. Dykman, *Journal of Quantitative Spectroscopy & Radiative Transfer*, 2010, **111**, 1-35.
30. H. W. Liao, C. L. Nehl and J. H. Hafner, *Nanomedicine*, 2006, **1**, 201-208.
31. M. Scampicchio, A. Arecchi and S. Mannino, *Nanotechnology*, 2009, **20**, -.
32. G. F. Wang, A. S. Stender, W. Sun and N. Fang, *Analyst*, 2010, **135**, 215-221.
33. D. A. Giljohann, D. S. Seferos, W. L. Daniel, M. D. Massich, P. C. Patel and C. A. Mirkin, *Angewandte Chemie-International Edition*, 2010, **49**, 3280-3294.
34. J. Z. Zhang, *Journal of Physical Chemistry Letters*, 2010, **1**, 686-695.
35. M. De, P. S. Ghosh and V. M. Rotello, *Advanced Materials*, 2008, **20**, 4225-4241.
36. E. E. Connor, J. Mwamuka, A. Gole, C. J. Murphy and M. D. Wyatt, *Small*, 2005, **1**, 325-327.
37. C. J. Murphy, A. M. Gole, J. W. Stone, P. N. Sisco, A. M. Alkilany, E. C. Goldsmith and S. C. Baxter, *Accounts of Chemical Research*, 2008, **41**, 1721-1730.
38. K. Rahme, P. Vicendo, C. Ayela, C. Gaillard, B. Payre, C. Mingotaud and F. Gauffre, *Chemistry-a European Journal*, 2009, **15**, 11151-11159.
39. Y. J. Min, M. Akbulut, K. Kristiansen, Y. Golan and J. Israelachvili, *Nature Materials*, 2008, **7**, 527-538.
40. D. Walczyk, F. B. Bombelli, M. P. Monopoli, I. Lynch and K. A. Dawson, *Journal of the American Chemical Society*, 2010, **132**, 5761-5768.
41. S. Sistach, K. Rahme, N. Perignon, J. D. Marty, N. L. D. Viguerie, F. Gauffre and C. Mingotaud, *Chemistry of Materials*, 2008, **20**, 1221-1223.
42. C. Fang, N. Bhattarai, C. Sun and M. Q. Zhang, *Small*, 2009, **5**, 1637-1641.
43. R. Gref, M. Luck, P. Quellec, M. Marchand, E. Dellacherie, S. Harnisch, T. Blunk and R. H. Muller, *Colloids and Surfaces B-Biointerfaces*, 2000, **18**, 301-313.
44. N. Halas, *Mrs Bulletin*, 2005, **30**, 362-367.
45. W. Z. Lai, W. Zhao, R. Yang and X. G. Li, *Acta Physico-Chimica Sinica*, 2010, **26**, 1177-1183.
46. H. Furusho, K. Kitano, S. Hamaguchi and Y. Nagasaki, *Chemistry of Materials*, 2009, **21**, 3526-3535.
47. T. Teranishi, I. Kiyokawa and M. Miyake, *Advanced Materials*, 1998, **10**, 596-+.
48. O. Masala and R. Seshadri, *Annual Review of Materials Research*, 2004, **34**, 41-81.
49. K. Rahme, J. Oberdisse, R. Schweins, C. Gaillard, J. D. Marty, C. Mingotaud and F. Gauffre, *Chemphyschem*, 2008, **9**, 2230-2236.
50. C. W. Chu, J. S. Na and G. N. Parsons, *Journal of the American Chemical Society*, 2007, **129**, 2287-2296.
51. C. G. Wu, Hongyan Hu, Jiawen., *Acta Chim. Sinica,* , 2009, **67**, 1621-1625.
52. J. M. D. K. B. J. M. D. Dixon., *Gold Bull DOI 10.1007/s13404-011-0015-8*.
53. Y. L. Liu, M. K. Shipton, J. Ryan, E. D. Kaufman, S. Franzen and D. L. Feldheim, *Analytical Chemistry*, 2007, **79**, 2221-2229.
54. L. Jokerst, Zare & Gambhir, *Nanomedicine*, 2011, **6**, 715-728.
55. D. Miyamoto, M. Oishi, K. Kojima, K. Yoshimoto and Y. Nagasaki, *Langmuir*, 2008, **24**, 5010-5017.
56. U. I. Tromsdorf, O. T. Bruns, S. C. Salmen, U. Beisiegel and H. Weller, *Nano Letters*, 2009, **9**, 4434-4440.
57. T. Niidome, M. Yamagata, Y. Okamoto, Y. Akiyama, H. Takahashi, T. Kawano, Y. Katayama and Y. Niidome, *Journal of Controlled Release*, 2006, **114**, 343-347.
58. H. Otsuka, Y. Nagasaki and K. Kataoka, *Advanced Drug Delivery Reviews*, 2003, **55**, 403-419.
59. T. Merdan, K. Kunath, H. Petersen, U. Bakowsky, K. H. Voigt, J. Kopecek and T. Kissel, *Bioconjugate Chemistry*, 2005, **16**, 785-792.

60. B. C. Mei, K. Susumu, I. L. Medintz and H. Mattoussi, *Nature Protocols*, 2009, **4**, 412-423.
61. W. H. De Jong, W. I. Hagens, P. Krystek, M. C. Burger, A. J. A. M. Sips and R. E. Geertsma, *Biomaterials*, 2008, **29**, 1912-1919.
62. H. S. Choi, B. I. Ipe, P. Misra, J. H. Lee, M. G. Bawendi and J. V. Frangioni, *Nano Letters*, 2009, **9**, 2354-2359.
63. M. C. Wan-Seob Cho, Jinyoung Jeong et al., *Toxicology and Applied Pharmacology*, 2010, **245**, 116–123.
64. W. D. Zhang XD, Shen X, Chen J, Sun YM, Liu PX, Liang XJ, *Biomaterials*, 2012, **33**, 6408–6419.
65. G. D. Zhang, Z. Yang, W. Lu, R. Zhang, Q. Huang, M. Tian, L. Li, D. Liang and C. Li, *Biomaterials*, 2009, **30**, 1928-1936.
66. Z. e. al, *International Journal of Nanomedicine*, 2011, **6**, 2071–2081.
67. R. M. A.-M. S. Harakeh, P.R. Gil, R.A Sperling, A. Meinhardt, A. Niedzwiecki, M. Rath, W.J. Parak, E. Baydoun. , *Nanotoxicology*, 2010, **44**, 177-185.
68. N. K. a. L. Dykman, *Chem. Soc. Rev.*, 2011, **40**, 1647-1671.
69. S. A. Takae, Y.; Otsuka, H.; Nakamura, T.; Nagasaki, Y.; Kataoka, K. , *Biomacromolecules*, 2005, **6**, 818–824.
70. K. R. Brown and M. J. Natan, *Langmuir*, 1998, **14**, 726-728.
71. K. R. Brown, L. A. Lyon, A. P. Fox, B. D. Reiss and M. J. Natan, *Chemistry of Materials*, 2000, **12**, 314-323.
72. J. Rodriguez-Fernandez, J. Perez-Juste, F. J. G. de Abajo and L. M. Liz-Marzan, *Langmuir*, 2006, **22**, 7007-7010.
73. N. R. Jana, L. Gearheart and C. J. Murphy, *Langmuir*, 2001, **17**, 6782-6786.
74. K. R. Brown, D. G. Walter and M. J. Natan, *Chemistry of Materials*, 2000, **12**, 306-313.
75. X. Q. Zou, E. B. Ying and S. J. Dong, *Nanotechnology*, 2006, **17**, 4758-4764.
76. S. D. Perrault and W. C. W. Chan, *Journal of the American Chemical Society*, 2009, **131**, 17042-+.
77. J. Kimling, M. Maier, B. Okenve, V. Kotaidis, H. Ballot and A. Plech, *Journal of Physical Chemistry B*, 2006, **110**, 15700-15707.
78. J. Turkevich, P. C. Stevenson and J. Hillier, *Discuss. Faraday. Soc* 1951, **11**, 55-75.
79. G. Frens, *Nature-Physical Science*, 1973, **241**, 20-22.
80. K. T. Yong, M. T. Swihart, H. Ding and P. N. Prasad, *Plasmonics*, 2009, **4**, 79-93.
81. J. Polte, T. T. Ahner, F. Delissen, S. Sokolov, F. Emmerling, A. F. Thunemann and R. Kraehnert, *Journal of the American Chemical Society*, 2010, **132**, 1296-1301.
82. H. B. Xia, S. O. Bai, J. Hartmann and D. Y. Wang, *Langmuir*, 2010, **26**, 3585-3589.
83. X. H. Ji, X. N. Song, J. Li, Y. B. Bai, W. S. Yang and X. G. Peng, *Journal of the American Chemical Society*, 2007, **129**, 13939-13948.
84. T. K. Sau, A. Pal, N. R. Jana, Z. L. Wang and T. Pal, *Journal of Nanoparticle Research*, 2001, **3**, 257-261.
85. V. M. Gun'ko, A. V. Klyueva, Y. N. Levchuk and R. Leboda, *Advances in Colloid and Interface Science*, 2003, **105**, 201-328.
86. S. Takae, Y. Akiyama, H. Otsuka, T. Nakamura, Y. Nagasaki and K. Kataoka, *Biomacromolecules*, 2005, **6**, 818-824.
87. B. Shi, C. Fang and Y. Y. Pei, *Journal of Pharmaceutical Sciences*, 2006, **95**, 1873-1887.
88. W. P. Wuelfing, S. M. Gross, D. T. Miles and R. W. Murray, *Journal of the American Chemical Society*, 1998, **120**, 12696-12697.
89. S. J. Hurst, A. K. R. Lytton-Jean and C. A. Mirkin, *Analytical Chemistry*, 2006, **78**, 8313-8318.
90. L. Maus, J. P. Spatz and R. Fiammengo, *Langmuir*, 2009, **25**, 7910-7917.
91. P. D. Jadzinsky, G. Calero, C. J. Ackerson, D. A. Bushnell and R. D. Kornberg, *Science*, 2007, **318**, 430-433.
92. P. G. Degennes, *Adv. Colloid Interface Sci.*, 1987, **27**, 189–209.

93. PG Degennes, *Macromolecules* 1980, **13**, 1069–1075
94. A. H. d. V. wankyu Lee, Siewert-Jan Marrink, and Richard W. Pastor, *J. Phys. Chem. B*, 2009, **113**, 13186–13194.
95. M. W. M.Brust, D. Bethell, D.J. Schiffrin, R. Whyman *Journal of the Chemical Society Chemical Communications* 1994, **7**, 801.
96. C. D. Agnès Anne , and Jacques Moiroux, *Macromolecules*, 2002, **35**, 5578–5586.